Version 1.0 as of December 12, 2015

Lattice Study of Magnetic Catalysis in Graphene

Christopher Winterowd,[1] Carleton DeTar,[1] and Savvas Zafeiropoulos[2]

[1]*Department of Physics and Astronomy*
University of Utah, Salt Lake City, Utah, USA
[2]*Institut für Theoretische Physik - Johann Wolfgang Goethe-Universität*
Max-von-Laue-Str. 1, 60438 Frankfurt am Main, Germany

(Dated: December 12, 2015)

We discuss the simulation of the low energy effective field theory (EFT) for graphene in the presence of an external magnetic field. Our fully non-perturbative calculation uses methods of lattice gauge theory to study the theory using a Hybrid Monte Carlo approach. We investigate the phenomenon of magnetic catalysis in the context of graphene by studying the chiral condensate which is the order parameter for the symmetry breaking pattern $U(4) \to U(2) \otimes U(2)$. We also study the mass spectrum of the theory, in particular the Nambu-Goldstone (NG) mode as well as the Dirac quasiparticle which is predicted to obtain a dynamical mass. Finally we comment on the spectrum of the Dirac operator and what it tells us about magnetic catalysis.

PACS numbers:

I. INTRODUCTION

The experimental verification of graphene counts as one of the most important discoveries in recent years [1]. The field has seen tremendous growth in part due to the novel many-body and electronic properties of graphene [2]. In particular a host of developments have appeared in studying graphene in the presence of a magnetic field [3].

Graphene, a two-dimensional hexagonal lattice of Carbon atoms, has an unusual band structure consisting of a conduction and valence band that come together at two inequivalent points in the Brillouin zone. At these so called "Dirac points", the two bands take the shape of cones. The consequence of this band structure is that the low energy excitations are described by massless Dirac fermions. These Dirac fermions have a Fermi velocity that satisfies $v_F/c \approx 1/300$ and thus one does not have Lorentz invariance. Furthermore, this small velocity renders the interaction between the Dirac quasiparticles to be essentially Coulombic.

The strength of the interaction between the quasiparticles is affected by the substrate on which the graphene layer sits. For suspended graphene, the Coulomb interaction is unscreened and the analogue of the fine structure constant for graphene satisfies $\alpha_g \equiv e^2/\epsilon_0 v_F 4\pi > 1$. It is known that for sufficiently large coupling, the EFT undergoes a phase transition, as has been shown in several previous studies [4–7]. This transition is characterized by the appearance of a nonzero value of the condensate, $\langle\bar{\psi}\psi\rangle$, as well as a dynamic mass for the fermion.

In the presence of an external magnetic field, many field theories are thought to undergo spontaneous symmetry breaking. This phenomenon is known as magnetic catalysis and is posited to be universal. In the context of the graphene EFT, the magnetic catalysis scenario leads to the appearance of a dynamically generated Dirac mass and is proposed to account for one of the quantum Hall plateaus that appear at large magnetic field [8, 9].

The layout of this article is the following. In Section II we discuss the continuum EFT, its symmetries, as well as our lattice setup. In Section III we discuss the physics mechanism behind magnetic catalysis and review the results that apply to graphene. In Section V we discuss our results for the various condensate as well as the mass spectrum of the EFT. Finally, in Section VI, we conclude and discuss the interpretation of these results.

II. GRAPHENE EFT

A. Continuum

The continuum EFT describing the low energy properties of monolyaer graphene contains $N_f = 2$ species of four-component Dirac spinors in $(2+1)$ dimensions interacting via a Coulomb interaction. The counting of the fermionic degrees of freedom is as follows: 2 sublattices +2 Dirac points +2 spin projections of the electrons. The interaction is introduced via a scalar potential which lives in $(3+1)$ dimensions. The continuum action is given by

$$\begin{aligned} S &= \int dt d^2x \sum_{a=1,2} \bar{\psi}_a \not{D}[A_0] \psi_a \\ &+ \frac{\epsilon}{2e^2} \int dt d^3x \, (\partial_i A_0)^2, \end{aligned} \tag{1}$$

where the Dirac operator is given by

$$\not{D}[A_0] = \gamma_0 \left(\partial_0 + i A_0\right) + v_F \sum_{i=1,2} \gamma_i \partial_i. \tag{2}$$

Here we use a reducible representation of the gamma matrices in (2+1) dimensions, constructed from two inequiv-

alent reducible representations, which is given by

$$\gamma_\mu = \begin{pmatrix} \sigma_\mu & 0 \\ 0 & -\sigma_\mu \end{pmatrix}, \quad \mu = 0, 1, 2, \tag{3}$$

where $\sigma_0 \equiv \sigma_3$. In $(3+1)$ dimensions there is a similarity transformation, $S^\dagger \gamma_\mu S = -\gamma_\mu$, which relates the two representations with $S = \gamma_5$. Here, in $(2+1)$ dimensions, γ_5 nor chirality exist as $\prod_{\mu=0}^{2} \sigma_\mu \propto \mathbf{1}$. One can define a set of matrices which generate flavor transformations in the graphene EFT

$$\tilde{\gamma}_4 = \begin{pmatrix} 0 & \mathbf{1} \\ \mathbf{1} & 0 \end{pmatrix}, \quad \tilde{\gamma}_5 = \begin{pmatrix} 0 & \mathbf{1} \\ -\mathbf{1} & 0 \end{pmatrix}, \tag{4}$$

$$\tilde{\gamma}_{4,5} \equiv \tilde{\gamma}_4 \tilde{\gamma}_5 = \begin{pmatrix} -\mathbf{1} & 0 \\ 0 & \mathbf{1} \end{pmatrix}, \tag{5}$$

where $\{\tilde{\gamma}_4, \gamma_\mu\} = \{\tilde{\gamma}_5, \gamma_\mu\} = \{\tilde{\gamma}_4, \tilde{\gamma}_5\} = 0$.

The fermionic part of the action in (1) has a $U(4)$ symmetry whose generators are given by

$$\mathbf{1} \otimes \mathbf{1}, \quad \mathbf{1} \otimes \sigma_\mu, \quad \tilde{\gamma}_{4,5} \otimes \mathbf{1}, \quad \tilde{\gamma}_{4,5} \otimes \sigma_\mu \tag{6}$$

$$\tilde{\gamma}_4 \otimes \mathbf{1}, \quad \tilde{\gamma}_4 \otimes \sigma_\mu, \quad \tilde{\gamma}_5 \otimes \mathbf{1}, \quad \tilde{\gamma}_5 \otimes \sigma_\mu. \tag{7}$$

The appearance of a mass term of the form $m \sum_{a=1,2} \bar{\psi}_a \psi_a$ breaks the $U(4)$ symmetry down to $U(2) \otimes U(2)$ whose generators are given by (6). Thus, the formation of a nonzero value of the condensate $\langle \bar{\psi}_a \psi_a \rangle$, would signal spontaneous symmetry breaking and the appearance of 8 Nambu-Goldstone bosons. In Appendix (ref new appendix with information regarding condensate and spinor basis) we provide the details of our basis for the Dirac spinors and the various bilinear condensates that can occur. This helps clarify the meaning of field theoretic operators in terms of the original tight-binding model on the hexagonal lattice.

B. Lattice

Taking the continuum EFT, (1), which is valid up to some cutoff Λ, we now discretize it on a cubic lattice. It is important to emphasize that this lattice is not directly related to the original honeycomb lattice of graphene. Lattice methods in gauge theories have shown to be useful in elucidating the non-perturbative aspects of strongly interacting theories such as quantum chromodynamics (QCD) [10]. Thus, we chose to apply these methods to the study of the graphene EFT.

As expected, we represent the gauge potential, $A_0(n)$, via the variable $U_0(n) \equiv \exp(iaA_0(n))$, which lives on the links of the lattice. We take the fermion fields to live on the sites of the lattice. The discretization of the gauge action is as follows. We first write the action in terms of the $U(1)$-valued links as follows

$$S_G = \frac{1}{g^2} \sum_n \sum_{i=1}^{3} \left[1 - \mathrm{Re} U_i^{(p)}(n) \right], \tag{8}$$

$$U_i^{(p)}(n) = U_0(n) U_0^\dagger(n + \hat{i}), \tag{9}$$

which is known as the compact formulation of the $U(1)$ gauge action. To avoid complications arising from an unwanted bulk phase transition [11], one expands the links to quadratic order in the potential to obtain the so-called non-compact action

$$S_G^{(NC)} = a_s^3 a_t \frac{\beta}{2} \sum_n \sum_{i=1}^{3} \frac{1}{a_s^2} \left(\theta(n) - \theta(n + \hat{i}) \right)^2, \tag{10}$$

where $\beta = 1/g^2$ and the gauge field lives in $(3+1)$ dimensions. Using the dimensionless field $\hat{\theta}(n) = a_t \theta(n)$, we write the above action as

$$S_G^{(NC)} = \xi \frac{\beta}{2} \sum_n \sum_{i=1}^{3} \left(\hat{\theta}(n) - \hat{\theta}(n + \hat{i}) \right)^2, \tag{11}$$

where $\xi \equiv a_s/a_t$ is known as the anisotropy parameter. It controls the ratio of the spatial lattice spacing to the temporal lattice spacing.

The discretization of the fermions has well-known complications encoded in the Nielsen-Ninomiya no-go theorem [12]. Namely, one wants to remove unphysical "doubler" modes while still preserving some part of the continuum $U(4)$ flavor symmetry. The method we use in this study employs the staggered fermion formulation [13], which eliminates some of the doublers while preserving a remnant of $U(4)$. The staggered fermion action is as follows

$$\begin{aligned} S_F &= a_s^2 a_t \sum_n \Bigg[\frac{1}{2a_t} \bar{\chi}_n \left(U_0(n) \chi_{n+\hat{0}} - U_0^\dagger(n - \hat{0}) \chi_{n-\hat{0}} \right) \\ &+ \frac{1}{2a_s} v_F \sum_{i=1,2} \eta_i(n) \bar{\chi}_n \left(\chi_{n+\hat{i}} - \chi_{n-\hat{i}} \right) \\ &+ \bar{\chi}_n \chi_n \Bigg], \end{aligned} \tag{12}$$

where the fermions live in $(2+1)$ dimensions and $\eta_1(n) = (-1)^{n_0}$, $\eta_2(n) = (-1)^{n_0+n_1}$ are the Kawamoto-Smit phases which appear due to spin diagonalization of the naive fermion action. The fields χ and $\bar{\chi}$ are one-component Grassmann variables. We have introduced a mass term which explicitly breaks the symmetry but is needed in our simulations as an infrared regulator. We can also write the fermionic action in terms of the dimensionless variables $\hat{\bar{\chi}}_n = a_s \bar{\chi}_n$, $\hat{\chi}_n = a_s \chi_n$, $\hat{m} = a_t m$

$$\begin{aligned} S_F &= \sum_n \Bigg[\frac{1}{2} \hat{\bar{\chi}}_n \left(U_0(n) \hat{\chi}_{n+\hat{0}} - U_0^\dagger(n - \hat{0}) \hat{\chi}_{n-\hat{0}} \right) \\ &+ \frac{v_F}{2\xi} \sum_{i=1,2} \eta_i(n) \hat{\bar{\chi}}_n \left(\hat{\chi}_{n+\hat{i}} - \hat{\chi}_{n-\hat{i}} \right) \\ &+ \hat{m} \hat{\bar{\chi}}_n \hat{\chi}_n \Bigg]. \end{aligned} \tag{13}$$

where $\xi \equiv a_s/a_t$ is the lattice anisotropy parameter. In our simulations we have taken $\xi = 3v_F$. In $(2+1)$ dimensions, each flavor of staggered fermions represents

two identical four-component Dirac spinors. In lattice QCD simulations, this degree of freedom, commonly referred to as "taste", is unwanted and considerable effort goes into eliminating it. In our case, the taste degree of freedom is desirable as we are attempting to simulate two identical species of Dirac fermions representing the low energy excitations of graphene. The taste degree of freedom becomes more apparent once one performs a change of basis, the details of which are relegated to Appendix A. The action in (13) retains a remnant $U(1) \otimes U(1)_\epsilon$ symmetry, where the $U(1)_\epsilon$ symmetry is broken with the appearance of a nonzero value of the condensate, $\langle \bar{\chi}\chi \rangle$. Thus on the lattice, one expects there to be a single NG boson as a result of this type of spontaneous symmetry breaking.

Although staggered fermions have some advantages in that they are cheap to simulate and retain a remnant chiral symmetry, it is known that at finite lattice spacing the violation of taste symmetry can be significant. In the case of QCD, for example, simulations with unimproved staggered fermions on fine lattices ($a = 0.05$ fm) obtain splittings within the pion taste-multiplet ($O(100\text{MeV})$) which are on the order of the physical pion mass [14]. It was found that taste violations are a result of the exchange of high-momentum gluons [15]. These couplings are eliminated by a process of link "fattening", which replaces the links $U_\mu(n)$ with a combination of other paths that connect the site n with $n + \hat{\mu}$.

Another improvement which has proven useful in lattice QCD simulations is the so called tadpole improvement [16]. This program is motivated by the observation that new vertices, with no continuum analogue, appear in lattice perturbation theory. These vertices are suppressed by powers of the lattice spacing but can lead to UV divergent diagrams which cancel the lattice spacing dependence of the vertex. In the graphene EFT, the tadpole factor, u_0, is defined in the following way

$$u_0 = \left(\langle U^{(p)} \rangle \right)^{1/2}, \tag{14}$$

where $\langle U^{(p)} \rangle$ is the volume averaged expectation value of the space-time oriented plaquette. Tadpole improvement consists of dividing each link in the temporal direction by u_0. Thus, each fat link receives a factor $1/u_0^{L_t}$ where L_t is the number of steps the path takes in the temporal direction.

One can further improve the staggered fermion action by introducing a third-nearest neighbor hopping. This is known as the Naik term [17]. With an appropriate weighting of the nearest neighbor and the third-nearest neighbor terms, one can obtain an improved free dispersion relation. Thus, using all of the above-mentioned ingredients, one has a tadpole improved action which is free of discretization errors up to $O(a^2)$. This is what is known as the improved AsqTad action.

Although previous lattice studies have used various levels of improvement for staggered fermions [18, 19], further reducing taste violations by using the AsqTad action will hopefully come closer to realizing the continuum theory. We will investigate this further when looking at the Dirac spectrum to see the effects of taste splittings.

The introduction of an external magnetic field on the lattice proceeds in the following manner. In the continuum, a homogenous magnetic field perpendicular to the sheet of graphene can be described by the Landau gauge vector potential, $A_\mu = \delta_{\mu,2} B x_1$. The spatial links are similarily modified, with a special prescription at the boundary due to the periodic boundary conditions

$$U_y(n) = e^{i a_s^2 e B n_x}, \tag{15}$$

$$U_x(n) = \begin{cases} 1 & , n_x \neq N_x - 1 \\ e^{-i a_s e B N_x n_y} & , n_x = N_x - 1 \end{cases}. \tag{16}$$

Furthermore, the toroidal geometry demands that the total flux through the lattice be quantized as follows [20]

$$\Phi_b \equiv eB = 2\pi \frac{N_B}{L_s^2}, \tag{17}$$

where L_s is the lattice extent in the spatial direction in units of a_s and N_B is an integer in the range

$$0 \leq N_B \leq \frac{N_x N_y}{4}. \tag{18}$$

We note that the spatial links, which describe the external magnetic field, are static and are not updated during the sampling of the path integral.

III. MAGNETIC CATALYSIS

The phenomenon of magnetic catalysis is a fascinating example of dynamical symmetry breaking [21–24]. In this scenario, an external magnetic field acts as a catalyst for fermion-antifermion pairing, even if they are weakly coupled. First studied in the context of the Nambu-Jona-Lasinio model and quantum electrodynamics in both (2+1) and (3+1) dimensions, magnetic catalysis has been predicted to occur also for planar condensed matter systems, including graphene [25–27]. Although various perturbative approaches have been used to study magnetic catalysis in various settings, it is useful to apply lattice methods as one is able to take a fully nonperturbative approach.

One can begin to understand the mechanism responsible for magnetic catalysis by first considering free Dirac fermions in the presence of an external magnetic field. This mechanism involves a dimensional reduction, $D \to D-2$, due to the magnetic field [28]. The Dirac equation in $(2+1)$ dimensions is given by

$$(i\gamma^\mu \mathcal{D}_\mu - m)\psi = 0, \tag{19}$$

where $\mathcal{D}_\mu = \partial_\mu - ieA_\mu$ and the gauge field is in Landau gauge. Solving (19), one finds that the energy levels are given by

$$E_n = \pm\sqrt{2|eB|n + m^2}, \tag{20}$$

where $n = 0, 1, 2, \cdots$ is the Landau level index and is given by a combination of orbital and spin contributions, $n \equiv k + s_z + 1/2$. The Landau levels are highly degenerate, with a degeneracy of $|eB|/2\pi$ for $n = 0$ and $|eB|/\pi$ for $n > 0$. When the Dirac mass is smuch smaller than the magnetic scale, $m \ll \sqrt{|eB|}$, the low energy sector is completely dominated by the lowest Landau level. Furthermore, the levels at $E_0 = \pm m$ do no disperse which confirms the kinematic aspect of the reduction, (2+1) $\rightarrow$ (0+1), due to the presence of the magnetic field.

An interesting consequence of an external field on Dirac fermions in $(2+1)$ dimensions is spontaneous symmetry breaking characterized by the appearance of a nonzero value for the condensate, $\langle\bar{\psi}\psi\rangle$. One can calculate the free propagator in the presence of an external field [29] and use the result to arrive at [30, 31]

$$\langle\bar{\psi}\psi\rangle = -\frac{1}{2\pi}\left(m\sqrt{2eB}\zeta\left(\frac{1}{2}, 1 + \frac{m^2}{2eB}\right) + eB - 2m^2\right) \quad (21)$$

where $\zeta(s, a)$ is the Hurwitz zeta function. Taking the limit $m \rightarrow 0$ of (21), one obtains

$$\lim_{m\rightarrow 0_+} \langle\bar{\psi}\psi\rangle(B, m) = -\frac{eB}{2\pi}. \quad (22)$$

Of course, by introducing interactions, this result will be modified. Extending the idea of dimensional reduction and recalling the dependence of the bound state energy in one dimensions on the coupling [32], one expects

$$m_{dyn} \propto \alpha_g\sqrt{eB}. \quad (23)$$

The idea of dimensional reduction and the associated spontaneous symmetry breaking which occurs in magnetic catalysis seems at odds with the Mermin-Wagner-Coleman (MWC) theorem [33, 34]. The MWC theorem states that spontaneous symmetry breaking is not possible in less than $(2 + 1)$ dimensions. Thus, a reduction $(2+1) \rightarrow (0+1)$ would seem to preclude the possibility of spontaneous symmetry breaking. The resolution of this apparent contradiction is that the NG bosons, which are a consequence of spontaneous symmetry breaking due to Goldstone's theorem, are charge neutral and thus are not subject to the reduction. This is contrast to the fermions and antifermions which are charged and thus have their motion in the plane perpendicular to the magnetic field constrained.

In addition to the condensate that one normally considers when discussing chiral symmetry breaking, there are other condensates which can describe the ground state of the graphene EFT in the presence of a magnetic field. In our study we also consider a time-reversal odd condensate, $\langle\bar{\psi}(-\tilde{\gamma}_{4,5})\psi\rangle$. While the former condensate leads to a Dirac mass in the graphene EFT, the latter condensate gives rise to a Haldane mass [35]. The ground state for $\nu = 0$ filling is posited to support a nonzero value for both condensates. In this work we study the flux dependence of both condensates in the chiral and zero-temperature limits.

IV. SIMULATION DETAILS

The generation of our gauge configurations was performed using a $U(1)$ variant of the Φ-algorithm [36]. This algorithm falls under a broad class of algorithms collectively known as hybrid Monte Carlo (HMC) [37]. This procedure introduces a fictitious time variable, τ, and a real valued canonical momentum, π_n, which is conjugate to the gauge potential θ_n. One is then able to construct a molecular dynamics Hamiltonian

$$\mathcal{H}^{(MD)} = \frac{1}{2}\sum_n \pi_n^2 + S_E, \quad (24)$$

where the momentum term is a gaussian weight which factors out during the calculation of expectation values. The equations of motion are then derived which follow from conservation of the Hamiltonian in molecular dynamics time

$$\dot{\theta}_n \equiv \frac{d\theta_n}{d\tau} = \pi_n, \quad (25)$$

$$\dot{\pi}_n \equiv \frac{d\pi_n}{d\tau} = -\frac{\partial S_E}{\partial\theta_n}. \quad (26)$$

Integrating these equations over a time interval of length T one generates a new configuration which one either accepts or rejects based on a Metropolis step. In this study we have used the second order leapfrog method in integrating (25) and (26).

The main question one has when selecting an algorithm to simulate dynamical fermions is how to best deal with the fermion determinant. In our case, we are interested in simulating two continuum species and thus, for staggered fermions, one can take advantage of the even-odd symmetry of the staggered Dirac operator. Namely, one first introduces a complex pseudofermion field ϕ which lives at each site of the lattice. Based on the identity

$$\det(M^\dagger M) = \int \mathcal{D}\phi^\dagger\mathcal{D}\phi e^{-\phi^\dagger\left(M^\dagger M\right)^{-1}\phi}, \quad (27)$$

one can use the pseudofermions to write the fermion action by making the identification $M \equiv \not{D}_{st} + m$. Noting that $M^\dagger M$ decouples even and odd sites, the determinant on the LHS of (27) overcounts the number of degrees of freedom by a factor of two. This can be accounted for by restricting the pseudofermions to the even sites, for example.

The Φ-algorithm starts by generating a random complex field distributed according to (27). One can then integrate the equations of motion over a trajectory. Specifically, the difficult part in doing this is computing the "force" given by (26). More specifically we can write this expression as

$$\dot{\pi}_n = -\frac{\partial S_g}{\partial\theta_n} - \frac{\partial S_f}{\partial\theta_n}, \quad (28)$$

where the first term represents the gauge force and the second term represents the fermion force. Expressing the

fermion action in terms of $\phi, \phi^\dagger$ one has

$$F_n^{(f)} = -\frac{\partial}{\partial\theta_n}\left(\phi^\dagger \left(M^\dagger M\right)^{-1}\phi\right), \tag{29}$$

where the calculation of the derivative with respect to θ_n involves a significant amount of terms for the AsqTad action. The calculation of the fermion force also involves solving the linear system $\left(M^\dagger M\right) X = \phi$ which is performed with an iterative solver. The gauge force has a concise expression which can be obtained by differentiating (10) with respect to θ_n, which leads to

$$F_n^{(g)} = -\beta \sum_i \left(2\theta(n) - \theta(n+\hat{i}) - \theta(n-\hat{i})\right). \tag{30}$$

After each trajectory, the pseudofermion field ϕ and the gauge momenta are refreshed. This strategy has been known to improve the amount of phase space explored by the algorithm and goes under the name of refereshed HMC.

In our simulations we have taken the trajectory length to be 1 and varied the step size for a given ensemble in order to obtain an acceptance rate of 70%. We have taken measurements every 10 trajectories with approximately $200-250$ trajectories needed for each ensemble to equilibrate. For the flux $\Phi_B = 0.125$, we have generated approximately 200 configurations per ensemble while for the other three fluxes we have generated roughly 100 configurations.

V. RESULTS

In this section we will discuss the results of our calculations regarding magnetic catalysis in the graphene EFT. Using the lattice methods described above, we will attempt to characterize the symmetry breaking using various observables. Apart from the condensates defined above, we will also investigate the quasiparticle and pseudoscalar mass as well as the spectrum of the Dirac operator. Thus, using diverse methods which have been used to study chiral symmetry breaking in the context of QCD can be applied to the graphene EFT.

In the absence of an external magnetic field, the graphene EFT is known to contain two phases: a semimetal phase at weak coupling (large dielectric constant ϵ) and an insulating phase at strong coupling (small ϵ). In the language of chiral symmetry breaking, the semimetal phase corresponds to the chirally symmetric phase while the insulating phase corresponds to the broken phase. Various aspects of this transition were studied previously using lattice methods [4–6, 18]. The transition is believed to be of second order as indicated by the results in [5].

The situation changes as one turns on the external magnetic field. Namely, the β_c which determines the boundary between the two phases shifts to larger values. This has been shown previously in [38] where at fixed temperature, the authors obtained a phase diagram in the (B, ϵ)-plane. One would expect that the phase boundary has a temperature dependence, where at $T = 0$, the authors of [21–24, 26, 27] predict that an infinitesimal attraction between fermions and antifermions willl lead to pairing and thus magnetic catalysis.

We began our calculations be identifying the semimetal phase through a scan in β coupled with an investigation of the condensate's behavior as a function of the bare mass in the chiral limit. In the semimetal phase, one expects the behavior of $\langle\bar{\psi}\psi\rangle$ to be linear in the bare mass for small values of m. One can compare this with the behavior of $\langle\bar{\psi}\psi\rangle$ as a function of the bare mass when the external magnetic field is turned on. This is illustrated in Fig. 1 where one sees a strongly nonlinear behavior of the condensate as a function of m for the magnetic fluxes $\Phi_B = 0.125$ and $\Phi_B = 0.1875$.

However, just like the case at zero magnetic field, as the explicit symmetry breaking parameter is taken to zero, the condensate also goes to zero in the presence of an external magnetic field. Usually, this signals that the symmetry is being restored due to the finite spatial extent of the box. Referring to Fig. 2, one can see that this is not the case. For several sizes of the xy-plane, where the fermions are located, the condensate shows little variation. This can be explained by noting that the magnetic length, $l_B \equiv \sqrt{\hbar c/eB}$, which characterizes the quasiparticle's cyclotron orbit, satisfies $1 < l_B < L_s$, in units of a_s. We have also confirmed this indepedently by calculating the screening masses for the fermion quasiparticle and the pseudoscalar, which satisfy $M_s L_s > 1$.

Thermal effects are also known to play a role in lattice simulations due to the finite extent of the box. The temperature of the system is related to the temporal extent of the lattice, $T = 1/N_\tau a_t$. We have investigated the effects of finite temperature on the condensate which is illustrated in Fig. 3 where $\sigma(T/m)$ is plotted. When the temperature is large compared to the fermion mass, one can see that the condensate tends towards zero. On the other hand, when the temperature is small compared to the fermion mass, one can see that the condensate increases and tends asymptotically towards a nonzero value. The fact that magnetic catalysis is a property of the ground state of the Hamiltonian suggests that we first take the limit $T \to 0$ followed by the limit $m \to 0$. Using this strategy we have first extrapolated to zero temperature at a fixed bare fermion mass. We then use this points for our chiral extrapolation. This is illustrated in Fig. 4, where we plot the chiral limit of the $T = 0$ extrapolated points.

VI. CONCLUSION

Appendix A: Spin-Taste Basis in $(2+1)$ dimensions

In this appendix we discuss the spin taste basis in $(2+1)$ dimensions which has some differences with that

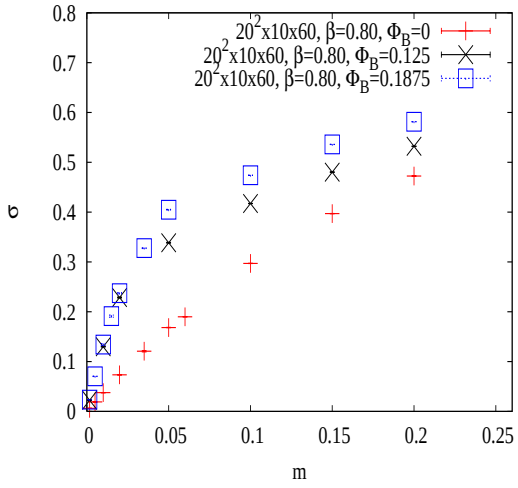

FIG. 1: $\sigma \equiv \langle\bar{\psi}\psi\rangle$ as a function of the bare fermion mass at zero field (red point) and at two values of the magnetic flux, $\Phi_B = 0.125$ (black points) and $\Phi_B = 0.1875$ (blue points) in units of a_s^2, as well as at zero external magnetic field (red points). One can note that σ vanishes with m at zero field as well as at nonzero external field. The vanishing of the condensate in the presence of the magnetic field is argued to be a thermal effect.

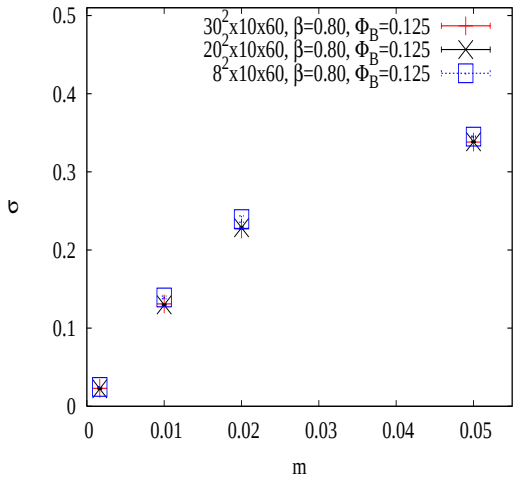

FIG. 2: σ as a function of fermion mass with varying spatial volume N_s^2 for magnetic flux $\Phi_B = 0.125$. The lattice volumes are listed in the form $N_s^2 \times N_z \times N_\tau$ where the fermions live in the xy-plane and the gauge field is present throughout the entire volume.

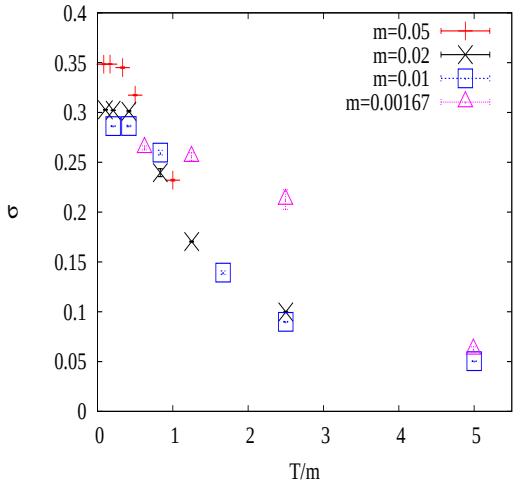

FIG. 3: σ plotted as a function of T/m. One can see that at small values of T/m, the condensate increases and tends towards a nonzero value.

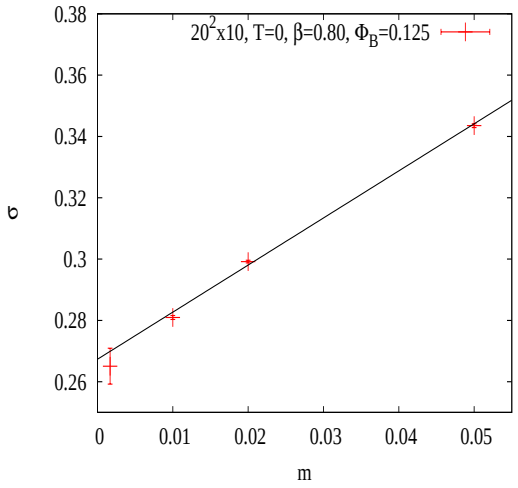

FIG. 4: Chiral limit of the condensate using the $T = 0$ extrapolated points.

of $(3+1)$ dimensions. The discussion follows that of [39]. Starting from the one-component fields $\chi, \bar{\chi}$ one performs a change of basis by introducing the following transformation

$$u^{\alpha a}(y) = \frac{1}{4\sqrt{2}} \sum_\eta \Gamma_\eta^{\alpha a} \chi_\eta(y), \qquad \text{(A1)}$$

$$d^{\alpha a}(y) = \frac{1}{4\sqrt{2}} \sum_\eta B_\eta^{\alpha a} \chi_\eta(y),$$

where one has introduced the matrices

$$\Gamma_\eta \equiv \sigma_0^{\eta_0}\sigma_1^{\eta_1}\sigma_2^{\eta_2}, \quad \text{(A2)}$$
$$B_\eta \equiv \beta_0^{\eta_0}\beta_1^{\eta_1}\beta_2^{\eta_2},\ \beta_\mu \equiv -\sigma_\mu, \quad \text{(A3)}$$

We note that one labels a lattice site by $n_\mu = 2y_\mu + \eta_\mu$, where y_μ is an integer that labels the corner of the cube and $\eta_\mu = 0, 1$ labels the sites within a cube. Using the identity $\mathrm{Tr}\,(\Gamma_\eta^\dagger\Gamma_{\eta'} + B_\eta^\dagger B_{\eta'}) = 4\delta_{\eta\eta'}$, one can invert the relation in (A1) to obtain

$$\chi_\eta(y) = \sqrt{2}\sum_{\alpha,a}(\Gamma_\eta^{*\alpha a}u^{\alpha a}(y) + B_\eta^{*\alpha a}d^{\alpha a}(y)), \quad \text{(A4)}$$
$$\bar\chi_\eta(y) = \sqrt{2}\sum_{\alpha,a}(\bar u^{\alpha a}(y)\Gamma_\eta^{\alpha a} + \bar d^{\alpha a}(y)B_\eta^{\alpha a}).$$

One can then rewrite the action in the spin-taste basis. For example, the mass term becomes

$$a^3 m\sum_{y,\eta}\bar\chi_\eta(y)\chi_\eta(y) = \quad \text{(A5)}$$
$$(2a)^3\sum_y\left(\bar u(y)(\mathbf{1}\otimes\mathbf{1})u(y) + \bar d(y)(\mathbf{1}\otimes\mathbf{1})d(y)\right),$$

where we have used the following identities

$$\sum_\eta \Gamma_\eta^{\alpha a}\Gamma_\eta^{*\beta b} = \sum_\eta B_\eta^{\alpha a}B_\eta^{*\beta b} = 4\delta_{\alpha\beta}\delta_{ab}, \quad \text{(A6)}$$
$$\sum_\eta \Gamma_\eta^{\alpha a}B_\eta^{*\beta b} = 0. \quad \text{(A7)}$$

To rewrite the kinetic term one first expresses the shifted field as

$$\chi_{\eta+\hat\mu}(y) = \delta_{\eta_\mu,0}\eta_\mu(\eta)\sqrt{2}\,\mathrm{Tr}\left(\Gamma_\eta^\dagger\gamma_\mu u(y) + B_\eta^\dagger\beta_\mu d(y)\right) \quad \text{(A8)}$$
$$+\delta_{\eta_\mu,1}\eta_\mu(\eta)\sqrt{2}\,\mathrm{Tr}\left(\Gamma_\eta^\dagger\gamma_\mu u(y+\hat\mu) + B_\eta^\dagger\beta_\mu d(y+\hat\mu)\right).$$

A similar expression exists for the backward shifted field, $\chi_{\eta-\hat\mu}(y)$, and thus one arrives at the following form for the staggered action

$$S_{st} = (2a)^3\sum_{y,\mu}\Big\{\bar u(y)(\gamma_\mu\otimes\mathbf{1})\partial_\mu u(y) + \bar d(y)(\beta_\mu\otimes\mathbf{1})\partial_\mu d(y)$$
$$+ a[\bar u(y)(\mathbf{1}\otimes\gamma_\mu^T)\partial_\mu^2 d(y) + \bar d(y)(\mathbf{1}\otimes\beta_\mu^T)\partial_\mu^2 u(y)]\Big\}$$
$$+ (2a)^3 m\sum_y[\bar u(y)(\mathbf{1}\otimes\mathbf{1})u(y) + \bar d(y)(\mathbf{1}\otimes\mathbf{1})d(y)], \quad \text{(A9)}$$

where γ_μ^T refers to the transpose and derivative operators now act on a lattice of spacing $2a$. One can now define a four-component Dirac spinor as follows

$$\Psi(y) = \begin{pmatrix} u(y) \\ d(y)\end{pmatrix}. \quad \text{(A10)}$$

Using the reducible set of gamma matrices in (3) and (4) one can write the action in the following compact form

$$S_{st} = (2a)^3\sum_{y,\mu}\Big\{\bar\Psi(y)(\gamma_\mu\otimes\mathbf{1})\partial_\mu\Psi(y) \quad \text{(A11)}$$
$$+ a\bar\Psi(y)(\tilde\gamma_5\otimes\gamma_\mu^T)\partial_\mu^2\Psi(y)\Big\}$$
$$+ (2a)^3 m\sum_y\bar\Psi(y)(\mathbf{1}\otimes\mathbf{1})\Psi(y).$$

One sees from (A11) that the second derivative term, which is suppressed by a factor of the lattice spacing, is not invariant under a rotation in taste space.

The residual symmetry of the staggered lattice action is $U(1)\otimes U(1)_\epsilon$. The form of these symmetries on the one-component fields is as follows

$$\chi(x) \to \exp(i\alpha)\chi(x),$$
$$\bar\chi(x) \to \bar\chi(x)\exp(-i\alpha), \quad \text{(A12)}$$
$$\chi(x) \to \exp(i\beta\epsilon(x))\chi(x),$$
$$\bar\chi(x) \to \bar\chi(x)\exp(i\beta\epsilon(x)), \quad \text{(A13)}$$

where $\epsilon(x) \equiv (-1)^{x_0+x_1+x_2}$. In terms of the fields u and d these transformations become

$$\begin{pmatrix} u \\ d\end{pmatrix} \to \exp(i\alpha)\begin{pmatrix} u \\ d\end{pmatrix},$$
$$\begin{pmatrix} \bar u & \bar d\end{pmatrix} \to \begin{pmatrix} \bar u & \bar d\end{pmatrix}\exp(-i\alpha), \quad \text{(A14)}$$
$$\begin{pmatrix} u \\ d\end{pmatrix} \to \begin{pmatrix} \cos(\beta) & i\sin(\beta) \\ i\sin(\beta) & \cos(\beta)\end{pmatrix}\begin{pmatrix} u \\ d\end{pmatrix},$$
$$\begin{pmatrix} \bar u & \bar d\end{pmatrix} \to \begin{pmatrix} \bar u & \bar d\end{pmatrix}\begin{pmatrix} \cos(\beta) & i\sin(\beta) \\ i\sin(\beta) & \cos(\beta)\end{pmatrix}. \quad \text{(A15)}$$

Thus, one can see that the formation of a condensate spontaneously breaks the $U(1)_\epsilon$ symmetry and leads to the appearance of a single NG boson.

Appendix A: Notation for Fermionic Observables

The graphene EFT describes two species of four-component Dirac spinors which are organized as follows

$$\Psi_\sigma^\top = (\psi_{\kappa A\sigma}, \psi_{\kappa B\sigma}, \psi_{\kappa' B\sigma}, \psi_{\kappa' A\sigma}), \quad \text{(A1)}$$

where κ, κ' refer to the Dirac points, σ refers to the electron's spin projection, and A, B refer to the sublattice. The Hamiltonian describing the dynamics of the low-energy EFT is given by

$$\mathcal{H} = v_F\int d\vec r\,\bar\Psi(\vec r)\,(\gamma_1\pi_x + \gamma_2\pi_y)\,\Psi(\vec r)$$
$$+ \int d\vec r\int d\vec r\,'\hat\rho\,(\vec r)\,\frac{e^2}{\epsilon|\vec r - \vec r\,'|}\hat\rho\,(\vec r\,'), \quad \text{(A2)}$$

where $\bar\Psi \equiv \Psi^\dagger\gamma_0$, $\hat\rho\,(\vec r) \equiv \Psi^\dagger(\vec r)\Psi(\vec r)$, ϵ is the dielectric constant of the substrate, and the gamma matrices are

defined in (3). As we have mentioned, the Hamiltonian in (A2) is diagonal in spin space and has a $U(4)$ symmetry described by the generators in (6) and (7). These generators have the four-dimensional sublattice $\otimes$ valley subspace tensored with the two-dimensional spin subspace. Although our lattice simulations do not take this into account, in real graphene this $U(4)$ symmetry is explicitly broken in the presence of an external magnetic field by the Zeeman term

$$\mathcal{H}_Z = -\int d\vec{r}\mu_B \Psi^\dagger \sigma_3 \Psi, \tag{A3}$$

where σ_3 acts in spin space. This term breaks the $U(4)$ symmetry down to $U(2)_\uparrow \times U(2)_\downarrow$ where the generators of $U(2)_\sigma$ are given by

$$\mathbf{1} \otimes P_\sigma, \quad \tilde{\gamma}_4 \otimes P_\sigma, \quad i\tilde{\gamma}_5 \otimes P_\sigma, \quad -\tilde{\gamma}_{4,5} \otimes P_\sigma, \tag{A4}$$

where we have introduced the spin projection operator, $P_\sigma \equiv \frac{1}{2}(1 \pm \sigma_3)$. Apart from the long-range Coulomb interaction present in (A2), in the complete lattice theory there are numerous short-range interactions which can have a decisive effect on the selection of the ground state [40]. Renormalization effects can strengthen these short-range interactions so that they become much stronger than the Zeeman term. In our lattice gauge model, we only consider a long-range Coulomb interaction mediated by a scalar potential and ignore the Zeeman interaction as well as other lattice-scale interactions.

In our study we are looking for spontaneous symmetry breaking in the presence of an external magnetic field. Typically this will involve breaking of the $SU(2)_\sigma$ symmetry where $SU(2)_\sigma$ is a subgroup of $U(2)_\sigma$ which is described above. In this section we will examine various terms and their corresponding order parameters which characterize the symmetry breaking.

We first introduce the Dirac mass term

$$\tilde{\Delta}_\sigma \bar{\Psi} P_\sigma \Psi = \tilde{\Delta}_\sigma \Psi^\dagger \gamma_0 P_\sigma \Psi, \tag{A5}$$

which is a triplet with respect to spin and breaks $SU(2)_\sigma$ down to $U(1)_\sigma$ with the generator $-\tilde{\gamma}_{4,5} \otimes P_\sigma$. The corresponding order parameter for this term is $\langle \bar{\Psi} P_\sigma \Psi \rangle$ and written in terms of it's Bloch components it can be expressed as

$$\begin{aligned} \tilde{\Delta}_\sigma : \quad & \psi^\dagger_{\kappa A\sigma}\psi_{\kappa A\sigma} - \psi^\dagger_{\kappa B\sigma}\psi_{\kappa B\sigma} \\ + \quad & \psi^\dagger_{\kappa' A\sigma}\psi_{\kappa' A\sigma} - \psi^\dagger_{\kappa' B\sigma}\psi_{\kappa' B\sigma}. \end{aligned} \tag{A6}$$

This form is convenient as one can interpret a nonzero value for this order parameter as an imbalance of charge between the two sublattices, A and B. This corresponds to a charge density wave (CDW).

Another type of mass term is given by

$$\Delta_\sigma \bar{\Psi}(-\tilde{\gamma}_{4,5}) P_\sigma \Psi = \Delta_\sigma \Psi^\dagger \gamma_0 (-\tilde{\gamma}_{4,5}) P_\sigma \Psi, \tag{A7}$$

which is a singlet with respect to spin but is odd under time-reversal. This mass term is commonly referrred to as the Haldane mass [35]. The order parameter for the Haldane mass is $\langle \bar{\Psi}(-\tilde{\gamma}_{4,5}) P_\sigma \Psi \rangle$ and it's expression in terms of Bloch components is given by

$$\begin{aligned} \Delta_\sigma : \quad & \psi^\dagger_{\kappa A\sigma}\psi_{\kappa A\sigma} - \psi^\dagger_{\kappa' A\sigma}\psi_{\kappa' A\sigma} \\ - \quad & \psi^\dagger_{\kappa B\sigma}\psi_{\kappa B\sigma} + \psi^\dagger_{\kappa' B\sigma}\psi_{\kappa' B\sigma}. \end{aligned} \tag{A8}$$

These order parameters are associated with magnetic catalysis and there are definite predictions of how they behave as a function of coupling and magnetic field.

[1] K. S. Novoselov *et al.*, Science **306**, 666, (2004)
[2] A. H. Castro Neto *et al.*, Rev. Mod. Phys. **81**, 109 (2009)
[3] M. O. Goerbig, Rev. Mod. Phys. **83**, 1193 (2011)
[4] J. E. Drut and T. A. Lahde, Phys. Rev. Lett. **102**, 026802 (2009)
[5] J. E. Drut and T. A. Lahde, Phys. Rev. B**79**, 165425, (2009)
[6] W. Armour, S. Hands, and C. Strouthos, Phys. Rev. B**81**, 125105 (2010)
[7] W. Armour, S. Hands, and C. Strouthos, Phys. Rev. B**84**, 075123 (2011)
[8] Y. Zhang *et al.*, Phys. Rev. Lett. **96**, 136806 (2006)
[9] Z. Jiang, Y. Zhang, H. L. Stormer, and P. Kim, Phys. Rev. Lett. **99**, 106802 (2007)
[10] T. DeGrand and C. DeTar, *Lattice Methods for Quantum Chromodynamics*, World Scientific (2006)
[11] J. B. Kogut and C. G. Strouthos, Phys. Rev. D**71**, 094012 (2005)
[12] H. B. Nielsen and M. Ninomiya, Nucl. Phys. **185**, 20 (1981)
[13] J. B. Kogut and L. Susskind, Phys. Rev. D**9**, 3501 (1974)
[14] A. Bazavov *et al.*, Rev. Mod. Phys. **82**, 1349 (2010)
[15] K. Orginos, R. Sugar, and D. Toussaint, Phys. Rev. D**60**, 054503 (1999)
[16] G. P. Lepage and P. B. Mackenzie, Phys. Rev. D**48**, 2250 (1993)
[17] S. Naik, Nucl. Phys. B**316**, 238 (1989)
[18] J. Giedt, A. Skinner, and S. Nayak, Phys. Rev. B**83**, 045420 (2011)
[19] J. E. Drut, T. A. Lahde, and L. Suoranta, arXiv:1002,1273, (2010)
[20] M. H. Al-Hashimi and U. J. Wiese, Annals Phys. **324**, 343 (2009)
[21] V. Gusynin, V. Miransky, and I. Shovkovy, Phys. Rev. Lett. **73**, 3499 (1994)
[22] V. Gusynin, V. Miransky, and I. Shovkovy, Phys. Rev. B**349**, 477 (1995)
[23] V. Gusynin, V. Miransky, and I. Shovkovy, Phys. Rev. D**52**, 4718 (1995)
[24] V. Gusynin, V. Miransky, and I. Shovkovy, Nucl. Phys.

B**462**, 249 (1996)
[25] D. V. Khveshchenko, Phys. Rev. Lett. **87**, 206401 (2001)
[26] E. Gorbar, V. Gusynin, V. Miransky, and I. Shovkovy, Phys. Rev. B**66**, 045108 (2002)
[27] E. Gorbar, V. Gusynin, V. Miransky, and I. Shovkovy, Phys. Scripta T**146**, 014018 (2012)
[28] I. Shovkovy, *Lect. Notes Phys.* **871**, 13 (2013)
[29] J. S. Schwinger, Phys. Rev. **82**, 664 (1951)
[30] W. Dittrich and H. Gies, Phys. Lett. B**392**, 182 (1997)
[31] W. Dittrich and M. Reuter, *Effective Lagrangians in Quantum Electrodynamics*, Springer (1985)
[32] L. D. Landau and E. M. Lifshitz, *Quantum Mechanics: Non-Relativistic Theory, 2nd edn.*, Pergamon (1965)
[33] N. D. Mermin and H. Wagner, Phys. Rev. Lett. **17**, 1133 (1966)
[34] S. Coleman, Nucl. Phys. B**145**, 110 (1978)
[35] F. Haldane, Phys. Rev. Lett. **61**, 2015 (1988)
[36] S. A. Gottlieb, W. Liu, D. Toussaint, R. L. Renken, and R. L. Sugar, Phys. Rev. D**35**, 2531 (1987)
[37] S. Duane and J. B. Kogut, Phys. Rev. Lett. **55**, 2774 (1985)
[38] D. L. Boyda, V. V. Braguta, S. N. Valgushev, M. I. Polikarpov, and M. V. Ulybyshev, Phys. Rev. B**89**, 245404 (2014)
[39] C. Burden and A. N. Burkitt, Eur. Phys. Lett. **3**, 545 (1987)
[40] I. L. Aleiner, D. E. Kharzeev, and A. M. Tsvelik, Phys. Rev. B**76**, 195415 (2007)